Available online at https://jcupt.bupt.edu.cn

The Journal of China Universities of Posts and Telecommunications

April 2025, 32(2): 56 – 69

Epileptic seizure prediction based on three-dimensional feature matrix and TDCBAM-SENet

Chao Hao[1], Han Jinying[1] (✉), Liu Yongli[1], Wang Weibin[2]

1. School of Computer Science and Technology, Henan Polytechnic University, Jiaozuo 454003, China
2. Beijing Shindata Technology Company, Beijing 100020, China

Abstract

Accurate prediction of epileptic seizures based on electroencephalogram (EEG) can assist doctors in taking timely treatment measures for patients. Previous prediction methods almost ignored the interaction and correlation among channels and the spatial domain information of multi-channel electrode positions, which may contain salient information related to epileptic states. A two-dimensional (2D) convolutional block attention module (CBAM) based squeeze-excitation (SE) network (TDCBAM-SENet) was proposed in this paper. Firstly, the time-frequency (TF) domain features of multi-channel EEG signal are utilized to design a three-dimensional (3D) matrix according to the relative positions of electrode channels. Then, the 2D CBAM (TDCBAM) is proposed to extract the high-level abstract features of salient information within channels by the channel attention module (CAM) and spatial location features by the spatial attention module (SAM). In addition, the SE model dynamically adjusts the weight of channels based on the spatial position information to capture the interaction information among channels. Finally, a multi-layer perceptron is introduced for classification. The CHB-MIT dataset is employed to evaluate the TDCBAM-SENet. Experimental results demonstrate that the 3D feature matrix effectively represents epilepsy salient information within and between EEG channels, and the TDCBAM-SENet can efficaciously mine the high-level abstract features of these information for epilepsy prediction.

Keywords seizure prediction, electroencephalogram (EEG), channel spatial location, epilepsy

1 Introduction

Epilepsy is a disease caused by the sudden abnormal discharge of brain cells, affecting approximately 50 million people worldwide[1]. Due to the different starting sites and transmission modes of abnormal electrical activity in the brain, the clinical manifestations of epilepsy are complex and diverse. This problem attracts the attention of researchers, it also brings certain challenges to the field of biomedical signal processing[2]. EEG places multiple electrodes in different parts of the brain based on voltage fluctuations, which identify and record electrical activity in the brain and detect signs of abnormal discharges. The feasibility and effectiveness of EEG-based seizure prediction are confirmed[3].

One of the important challenges for EEG seizure prediction is extracting discriminative EEG features of

Special Issue: The 27th Annual Meeting of The China Association for Science and Technology
Corresponding author: Han Jinying
E-mail: 1376594781@qq.com
DOI: 10.19682/j.cnki.1005-8885.2025.0010

the epileptic activity. Sun et al. proposed a channel attention method to fuse spatiotemporal features, which enables simultaneous acquisition of temporal information, spectral information, and spatial position information in EEG signals[4]. In addition, convolutional neural networks (CNN) and bi-directional long short-term memory (Bi-LSTM) are employed to extract features representing channel spatial position information and temporal information in EEG signals[5]. Zhong et al. proposed a 2D feature selection algorithm to eliminate unnecessary redundant features, which employed support vector machines (SVM) for accurate classification[6]. Furthermore, Feizbakhsh et al. clustered EEG signals in phase space, which ensured that the data density within each cluster is suitable for classification[7]. In addition, Ra et al. enhanced the TF resolution of EEG features using synchro extracting transformation and singular value decomposition (SET-SVD), followed by the utilization of CNN for seizure state classification[8]. Ozcan et al. merged hand-crafted features extracted from prior knowledge with hidden deep features, and fed the combined features into a multiplicative long short-term memory (MLSTM) to delve into the time-series dependencies of EEG[9]. Xu et al. utilized soft threshold denoising and an attention mechanism within the neural network to extract relevant features[10].

Currently, the most common deep model for epilepsy prediction based on EEG signals is CNN. Li et al. input the TF features into an alternating structure to model local features and long-range dependencies, which combines the complementary advantages of CNN and transformer[11]. Shi et al. developed an EEG preprocessing module using CNN and stochastic resonance effect[12]. This innovative module cannot only prevent the loss of EEG signals, but also provide information on different frequencies to improve the quality of EEG signals. Zhang et al. calculated Pearson correlation coefficients to obtain a correlation matrix, and used a lightweight CNN model to classify the correlation matrix[13]. In addition, in order to make use of the spectral representation of epilepsy rhythm, Ein Shoka et al. proposed a CNN-based transfer learning (TL) model, which encrypted 2D spectrogram images transformed by EEG time series, and fed them into the model for classification and prediction[14]. As mentioned above, although CNN has made some progress in the existing research, there are still some shortcomings. Such as CNNs have difficulty tracking complex nonlinear structures[15], which can only learn low-dimensional spatial correlations between EEG channels[16]. In particular, when processing EEG data, there are limitations in dealing with high-dimensional time series data and long-distance dependencies between channels. To address the issues, in the latest research of epileptic seizure prediction, Wang et al. used the phase-locked value (PLV) in EEG data to construct the adjacency matrix of the graph edge[17]. Chen et al. developed the joint graph structure and representation learning network (JGRN) for joint optimization of patient specific temporal channel connection weights[18]. Dissanayake et al. proposed an epileptic seizure predictor independent of the subject to realize the prediction of epileptic seizures[19]. In order to fully extract the temporal information of epileptic EEG, Zhong et al. introduced differential entropy (DE) applied to spatially coupled reasoning in network topology to calculate the temporal correlation of EEG and generate graph nodes[20]. Li et al. proposed a time-spectrum compression and excitation scheme to reduce the information redundancy of high-dimensional features[21]. Li et al. designed a lightweight CNN architecture based on EEG data, and they reparameterized the modified Monte Carlo dropout (RepNet-MMCD) strategy to obtain multi-scale feature representation[22]. In addition, the power spectral density (PSD) is used to separate the periodic and aperiodic components of the signal using parametric methods[23].

Although the existing epilepsy prediction research has made great progress, there are still some challenges. Firstly, due to the volume conductivity effect, the reactions between two physically adjacent electrodes tend to be similar. During the process of epileptic state transition, the changes of EEG signals in

different brain regions are not synchronized. Therefore, the correlation between these channels may contain salient information that is beneficial for epilepsy prediction. In addition, preserving the position of EEG electrodes during feature extraction can also provide gain information for epilepsy prediction. However, the existing feature extraction methods focus on extracting discriminative features within the EEG channel, without considering the interaction and correlation among channels and the spatial domain information of multi-channel electrode positions. Secondly, traditional machine learning models, such as CNN and deep belief networks (DBN), cannot handle the correlation features among EEG channels in different brain regions and spatial information features of electrode channel position. Especially, these models only focus on shallow static EEG construction, without considering the introduction of channel spatial position information to guide the dynamic adjustment of connectivity between channels.

To address the above issues, TDCBAM-SENet for epilepsy seizure prediction was proposed in this paper. Firstly, the EEG signal is preprocessed by short-time Fourier transform (STFT), which decomposes the time domain signal into different frequency and time spectrum components. Secondly, a 3D TF feature matrix is constructed based on the arrangement of electrodes in the brain. The 3D feature matrix contains information related to seizure status within the channel as well as spatial position information of the electrode channel. This representation is closer to the actual brain response and can help reduce information redundancy. Finally, an improved CNN model based on the TDCBAM-SENet model was designed, aiming to represent the EEG features of epileptic activity through a channel-space weighted attention mechanism. TDCBAM-SENet not only makes full use of the significant information in the TF domain, and the spatial location information of electrode channels contained in the 3D feature matrix, but also dynamically adjusts the weights of channels based on the spatial location information of channels, which helps to enhance the network's modeling ability for long-term dependence on time series data.

2 Methodology

2.1 3D TF feature matrix

The changes in EEG signals in different brain regions are not consistent during the process of epileptic seizure signal conversion. Some studies find that retaining the position information of EEG electrodes can provide favorable information for seizure prediction[24-26]. Therefore, the 3D TF feature matrix can effectively capture this useful information.

Firstly, time-domain and frequency-domain features are extracted from EEG. The specific features include mean, peak, standard deviation, skewness, approximate entropy, and PSD. Among them, EEG signals are segmented through a 4 s nonoverlapping Hamming window, and each segmented signal forms a 3D feature matrix to obtain frequency-domain features.

Multiple patients use different electrodes when recording data, which increases the bias in data analysis. Therefore, six TF domain features are extracted from the 20 channels commonly used by the patients, FP1-F7, F7-T7, T7-P7, P7-O1, FP1-F3, F3-C3, C3-P3, P3-O1, FP2-F4, F4-C4, C4-P4, P4-O2, FP2-F8, F8-T8, T8-P8-0, P8-O2, FZ-CZ, CZ-PZ, P7-T7, and T7-FT9, the number of features per sample is 120.

The EEG wires in the CHB-MIT[1] dataset use bipolar leads and record the electrode difference between the two electrodes[27-29], so the channel position is set to be between the two electrodes. Fig. 1 shows the International 10/20 system and its mapping matrix. The upper part shows the distribution of cortical electrodes, with the pink ones indicating the electrodes used for EEG data in this paper. Among them, NASION represents the nasal root and INION represents the posterior occipital protrusion. In Fig. 1, Z represents the position of the electrode at the mid-line of the brain. The lower part is the mapping matrix, which has a size of 9×9 and uses only 18 channels. The pink positions in the matrix are filled

with the feature values between the corresponding two electrodes. Arrange each feature of all channels according to the mapping rules in Fig. 1, and construct a 3D feature matrix of 9 × 9 × 1. It can characterize the spatial information of the brain and the synchronous changes between brain regions.

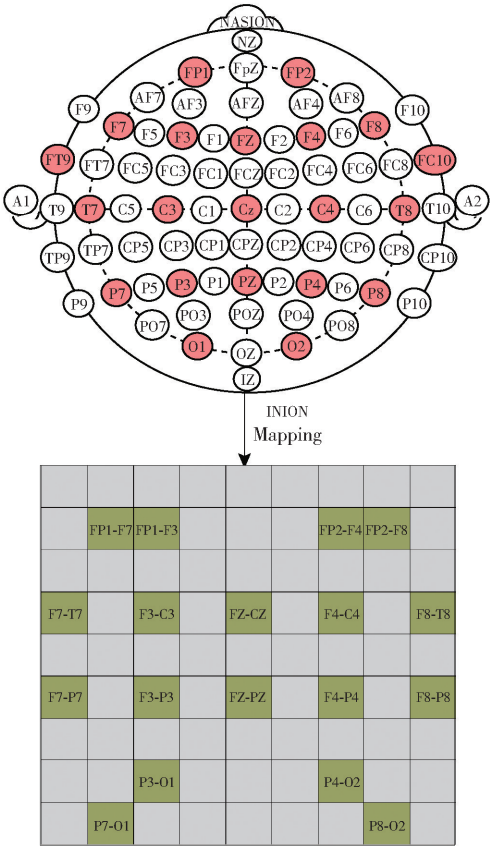

Fig. 1 International 10/20 system and 9 × 9 × 1 feature matrix

For each sample, a 9 × 9 × 1 3D feature matrix is constructed according to the mapping rules based on the six extracted TF domain features, as shown in Fig. 2. The 2D matrix mapped by the six TF domain features is merged into a 9 × 9 × 6 3D feature matrix in the third dimension.

In addition to the salient information related to epilepsy status within each channel, the constructed 3D matrix also contains the correlation information among EEG channels and the spatial domain information of the electrode channels.

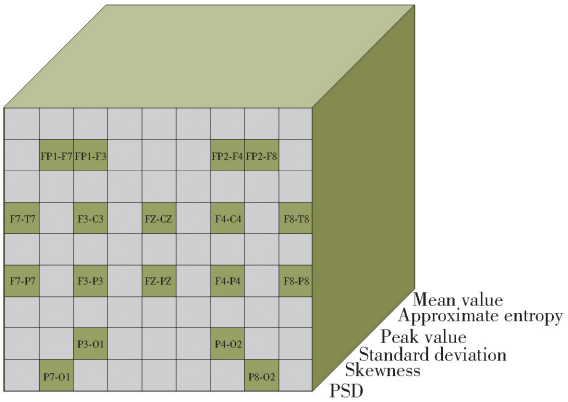

Fig. 2 3D TF feature matrix

2.2 TDCBAM-SENet model framework

The structure of the TDCBAM-SENet framework consists of convolutional modules, CBAMs, and a multilayer perceptron (MLP). The convolutional module contains four convolutional layers, each of which contains a rectified linear unit (ReLU) activation function, two dropout layers, and SE blocks, as shown in Fig. 3. In the framework, the input is the 3D feature matrix.

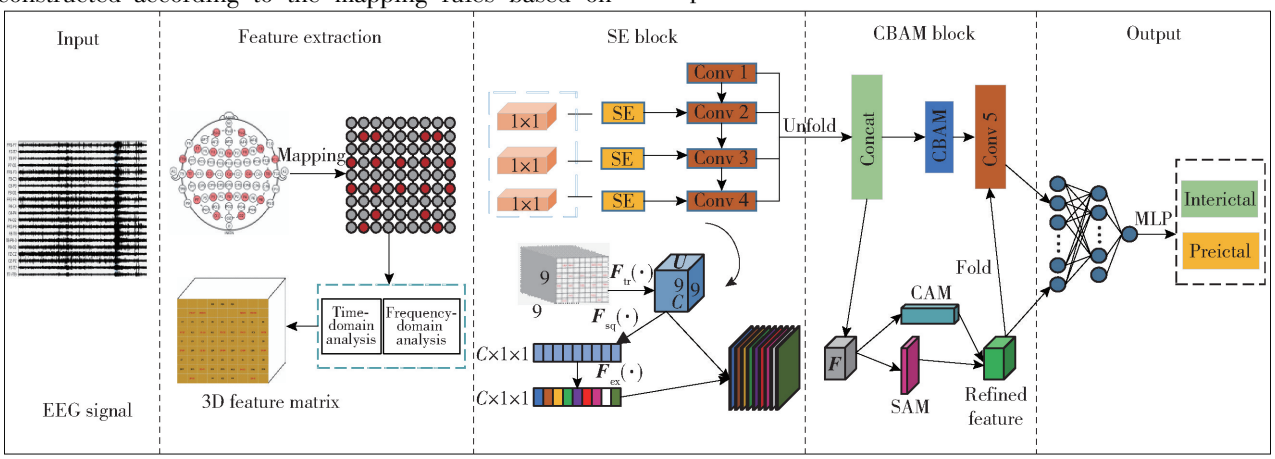

Fig. 3 Framework of the TDCBAM-SENet for seizure prediction

The SE block is in the convolution layer, assigning weights to each feature. The size of the receiving field depends on the size of the 3D feature matrix. Convolution is performed with different acceptance fields, which have an output dimension of 128. Epileptic states are classified by extracting epileptic features from the 3D matrix, performing SE operations in the 1 × 1 convolutional layer, and the matrix is input into the residual network block composed of Conv 1, Conv 2, Conv 3, and Conv 4, as shown in Fig. 3. It is combined with CBAM to weight features in the channel and spatial dimensions. The convolution operation of the model uses the ReLU activation function, and finally, the high-level abstract features extracted by the residual network block for classification. Two dropout layers and a softmax function are employed to output the seizure state, thereby preventing overfitting.

1) SE module

The SE module focuses on channel reationships. Considering that CBAM is not good at handling long-distance dependencies of features, an SE module is introduced. The SE module utilizes spatial position information in channels to dynamically adjust the weights of channels, which helps to enhance the network's modeling ability for long-range dependencies. The structure of the SE module is shown in Fig. 3.

The squeezing operation is performed first. The convolution operation is canceled, so $\boldsymbol{U}=[\boldsymbol{u}_1, \boldsymbol{u}_2, \ldots, \boldsymbol{u}_C]$, $C=6$ denotes the number of channels, $\boldsymbol{U} \in \mathbb{R}^{9\times9\times6}$. Among them, $\boldsymbol{u}_1$, $\boldsymbol{u}_2$, $\boldsymbol{u}_3$, $\boldsymbol{u}_4$, $\boldsymbol{u}_5$, and $\boldsymbol{u}_6$ represent 2D feature matrices composed of mean, peak, standard deviation, skewness, approximate entropy, and PSD. Then, the squeezing module incorporates the global information of the input data into the channel descriptor. This is achieved by global average pooling. The channel dependency description $\boldsymbol{Z}_C \in \mathbb{R}^6$, which is represented by $\boldsymbol{U}$ in 9×9 global average pooling generation on 9 dimensions. Therefore, the calculation of the $\boldsymbol{Z}_C$ is as follows. Among them, $\boldsymbol{F}_{sq}(\cdot)$ is the input square feature map with the shape of $C \times H \times W$, where H denotes the height, W denotes the width.

$$\boldsymbol{Z}_C=\boldsymbol{F}_{sq}(\boldsymbol{u}_C)=\frac{1}{H+W}\sum_{i=1}^{9}\sum_{j=1}^{9}\boldsymbol{u}_c(i,j); \quad c=1,2,\ldots,C \tag{1}$$

The excitation operation utilizes the information obtained from the squeeze operation to obtain complete dependence between EEG channels, which is achieved through two fully connected layers and two activation functions. This enables learning of nonlinear interactions between different features. Secondly, it focuses on all features rather than enforcing a single thermal activation. The excitation operation can be represented by

$$\boldsymbol{S}=\boldsymbol{F}_{ex}(\boldsymbol{Z}_C, W)=\sigma(\boldsymbol{g}(\boldsymbol{Z}_C, W))=\sigma(\boldsymbol{W}_2(\delta(\boldsymbol{W}_1\boldsymbol{Z}_C))) \tag{2}$$

where $\sigma(\cdot)$ is the sigmoid activation function and $\delta(\cdot)$ refers to the ReLU activation function. Among them, $\boldsymbol{F}_{ex}(\cdot)$ accepts the input $\boldsymbol{Z}_C$ and W, and outputs $\boldsymbol{S}$. $\boldsymbol{g}(\cdot)$ represents an intermediate function that accepts the input $\boldsymbol{Z}_C$ and W. $\boldsymbol{W}_1$ and $\boldsymbol{W}_2$ represent the weight matrices of the two linear transformations, respectively.

The operation of weight assignment is completed by the operation of colorization and excitation. In back propagation, the ReLU and sigmoid activation functions are used to update the weight parameters, strengthen the features that play a larger role in classification, and weaken the features that play a smaller role, the squeeze operation places the global information of the input feature matrix into the channel descriptor $\boldsymbol{Z}_C \in \mathbb{R}^C$. Therefore, the squeeze operation combines the contextual information of different convolution kernels in $\boldsymbol{F}_{tr}(\cdot)$. The convolutional network avoids focusing only on information in the receptive field of convolution kernels.

2) TDCBAM module

The TDCBAM module has two consecutive independent sub-modules, the CAM and the SAM, which strengthens important channel position information by weighting and reorganizing the feature matrix of electrode channel positions. The feature matrix is refined adaptively through CBAM in each convolutional block of the deep network. By utilizing

the SE block of channel attention, which focuses on the relationship between channels, these two methods can be combined to extract high-level abstract features in 2D CNN. This not only saves parameters and computational power, but also ensures that it can be integrated into existing network architectures as a plug-and-play module.

The structure of the CAM is shown in Fig. 4. Average pooling (AvgPool), $A(\cdot)$, and maximum pooling (MaxPool), $M(\cdot)$, operations are performed to aggregate spatial information in the 3D feature matrix, two different spatial context descriptors are generated: $\boldsymbol{F}^{\mathrm{C}}_{\mathrm{avg}}$ and $\boldsymbol{F}^{\mathrm{C}}_{\mathrm{max}}$, which represent the AvgPool feature and the MaxPool feature of the channel, obtaining a vector of the channel dimension, $C\times1\times1$. Both of these descriptors are fed back to the shared network to generate the channel attention matrix $\boldsymbol{M}_{\mathrm{C}}(\cdot)\in\mathbb{R}^{C\times1\times1}$. The shared network consists of a MLP with one hidden layer. To reduce parameter overhead, the hidden activation size is set to $(C/r)\times1\times1$, where r is the reduction ratio. After applying the shared network to each descriptor, the output feature vectors are combined using element wise summation. In short, the channel attention calculation is

$$\boldsymbol{M}_{\mathrm{C}}(\boldsymbol{F})=\sigma(\boldsymbol{M}_{\mathrm{lp}}(A(\boldsymbol{F}))+\boldsymbol{M}_{\mathrm{lp}}(M(\boldsymbol{F})))=\sigma(\boldsymbol{W}_1(\boldsymbol{W}_0(\boldsymbol{F}^{\mathrm{C}}_{\mathrm{avg}}))+\boldsymbol{W}_1(\boldsymbol{W}_0(\boldsymbol{F}^{\mathrm{C}}_{\mathrm{max}}))) \quad (3)$$

where $\sigma(\cdot)$ represents the sigmoid function, $\boldsymbol{W}_0\in\mathbb{R}^{C/(r\times C)}$, $\boldsymbol{W}_1\in\mathbb{R}^{(C\times C)/r}$. The two inputs share the $\boldsymbol{M}_{\mathrm{lp}}(\cdot)$ weights $\boldsymbol{W}_0$ and $\boldsymbol{W}_1$, and the ReLU activation function is followed by $\boldsymbol{W}_0$.

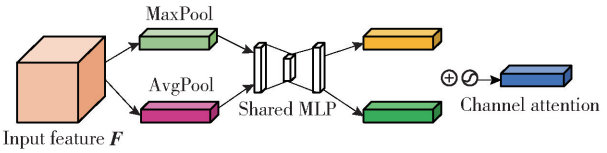

Fig. 4 Structure of CAM

In addition, spatial attention matrices are generated by utilizing the relationship between the positions of EEG channels. The structure of the SAM is shown in Fig. 5. To calculate SAM, AvgPool and MaxPool operations are applied along the channel axis, which are concatenated to generate valid feature descriptors $\boldsymbol{F}^{\mathrm{S}}_{\mathrm{avg}}$ and $\boldsymbol{F}^{\mathrm{S}}_{\mathrm{max}}$. By using these two pooling operations to aggregate the channel information of the features, it can effectively highlight the information. The spatial attention calculation process is

$$\boldsymbol{M}_{\mathrm{S}}(\boldsymbol{F})=\sigma(\boldsymbol{f}^{9\times9}(A(\boldsymbol{F})\oplus M(\boldsymbol{F})))=\sigma(\boldsymbol{f}^{9\times9}(\boldsymbol{F}^{\mathrm{S}}_{\mathrm{avg}}\oplus\boldsymbol{F}^{\mathrm{S}}_{\mathrm{max}})) \quad (4)$$

where $\oplus$ denotes the feature fusion operation. σ represents the sigmoid function and $\boldsymbol{f}^{9\times9}(\cdot)$ represents the convolution operation with a filter size of 9×9. $A(\boldsymbol{F})$ is the spatial attention map and $M(\boldsymbol{F})$ is the channel attention map.

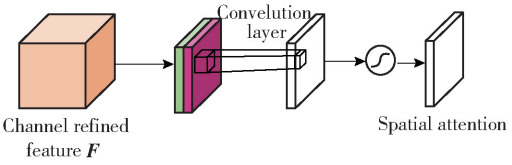

Fig. 5 Structure of SAM

Six given TF domain features form a 3D feature matrix, which are input into two attention modules to calculate complementary attention of channel features and spatial position features.

CBAM mainly focuses on the channels of features to improve the model's attention to different channels in features. The SE module re-calibrates the channel weights of the input feature matrix through global information, so that important channels are enhanced. Therefore, they can jointly optimize the representation of features at the channel level and global level, which makes the model more effective in learning the characteristics of the data. This combination can help the model better capture the correlations between data features, which improves the performance of the network, and can be widely applied to improve the representation ability of convolution.

3 Experiment and result analysis

3.1 Dataset and preprocessing

1) CHB-MIT dataset

In this paper, the public CHB-MIT dataset is utilized to evaluate the TDCBAM-SENet. The dataset consists of scalp EEG recordings from children with refractory epilepsy. It contains 23 recordings from 22

subjects, all of them are collected using the 10 – 20 international standard electrode placement. The EEG recordings are recorded using 18/23 leads, using a bipolar lead method. The start and end time of each epileptic seizure is marked in detail in this dataset. The sampling frequency and resolution are 256 Hz and 16 bit, respectively. The dataset includes a continuous scalp EEG recording of up to 967. 85 h, including 178 seizures. Due to the requirements of model training and testing, and considering that the number of interictal data samples is much larger than that of preictal data samples, the resampling methods is adopted to generate more training datasets to deal with the imbalance problem of data. In this experiment, 11 patients with epilepsy are selected, the number of epileptic seizures cannot be less than 3 times and cannot exceed 10 times.

2) Preprocessing

According to the seizure characteristics and duration in the EEG data of patients, the seizure period is divided into three parts, interictal, preictal, and postictal periods, that is three categories. Each part is segmented by time, and each segmented EEG is a sample, which inherits the category label of its part. The duration of the time window is 4 s, and no adjacent windows overlap. Specifically, 450 samples are selected from the samples contained in the preictal period and retained, 300 samples are selected from the samples contained in the interictal period to be retained. The TDCBAM-SENet is used to extract features from the dataset.

When collecting EEG signals, it is easy to be disturbed by other artificial noises, such as electromyogram (EMG) artifacts and EMG interference. Collecting raw EEG signals on the cerebral cortex can introduce noise interference in the human body, such as electrooculogram (EOG) artifacts and EOG interference. Therefore, in order to better extract EEG features, it is necessary to conduct noise reduction processing. The Fourier transform is employed to convert EEG signals into spectrograms. The band-stop filters and the high-pass filters are adopted to eliminate the 57 – 63 Hz and 117 – 123 Hz frequency components, while also removing the 0 direct current (DC) component. The spectrum obtained from the EEG signal after the above processing is shown in Figs. 6 and 7.

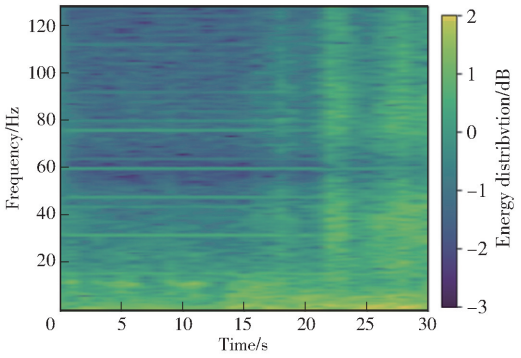

Fig. 6 Spectrum during the interictal period of seizures

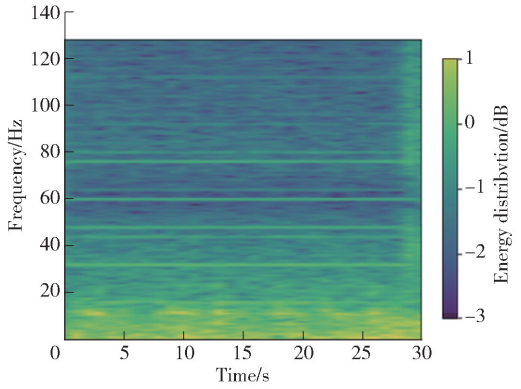

Fig. 7 Spectrum during the preictal period of seizures

3. 2 Experimental setup

1) 55 seizure records from 11 patients are selected from the CHB-MIT dataset, as shown in Table 1.

Table 1 Epileptic seizure records in 11 patients on CHB-MIT dataset

No. patient	Sex	Age	Number	Time/h
Chb01	Female	11. 0	7	45. 0
Chb02	Male	11. 0	3	39. 6
Chb03	Female	14. 0	7	57. 9
Chb04	Male	22. 0	4	154. 4
Chb05	Female	7. 0	5	38. 1
Chb07	Female	14. 5	3	67. 2
Chb08	Male	3. 5	5	26. 4
Chb10	Male	3. 0	7	72. 5
Chb11	Female	12. 0	3	73. 3
Chb21	Female	13. 0	4	55. 7
Chb23	Female	6. 0	7	70. 9

The EEG signals of epileptic patients are divided

into three periods, as shown in Fig. 8. Fig. 8 depicts epileptic signals from 20 electrod channels shared among 11 patients. Channels T7-P7 and T7-FT9 are omitted due to consistency across. The continuous EEG signals from 5 min to 30 min before the ictal of seizures are used as the preictal signals. The period of an epileptic seizure is regarded as the seizure ictal period. The period between the end of seizures and the beginning of the next seizure is defined as the interictal period.

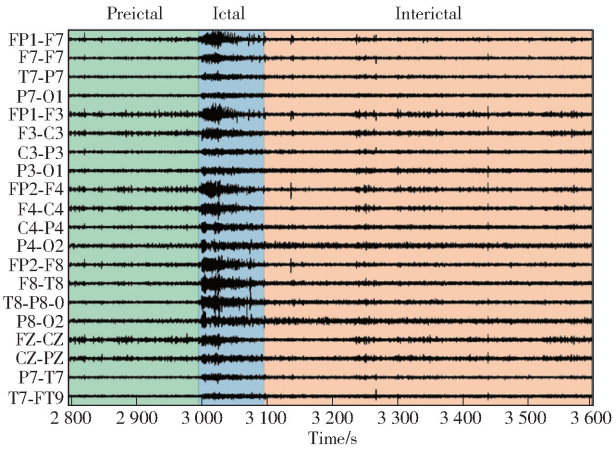

Fig. 8 Seizure state of EEG in epilepsy patients

Extract EEG features from the CHB-MIT dataset, the preictal period of each seizure record is defined as 1 800 s, and the interictal period is defined as 1 200 s. Setting every 4 s as a sample, so that 450 and 300 samples can be obtained for the preictal and interictal periods in each seizure record, respectively. The TF domain features of 18 channel EEG signals are extracted from each sample.

2) The BONN[8] dataset consists of 5 data subsets, namely F, S, N, Z, and O. Each of these sub-datasets contains 100 data fragments, each with a duration of 23.6 s. As can be seen from Table 2, the datasets Z and O are scalp EEG information of 5 healthy people, which constituted the comparison group. The fragment in Z dataset is EEG when the subject's eyes are open, and the fragment in O dataset is EEG when the subject's eyes are closed. The dataets N, F, and S are intracranial EEG collected from 5 patients with epilepsy, N and F are collected during the interictal period, and S is collected during the seizure period.

Table 2 BONN dataset

Subset	Status	Evaluate state	Record resource
Z	Normal	Eye open	Surface electrode
O	Normal	Eye closed	Surface electrode
N	Patient	Interictal	Inner electrode
F	Patient	Interictal	Inner electrode
S	Patient	Seizure	Inner electrode

Each BONN dataset contains 500 single channel i-EEG records, for 500 records. The time length of each data fragment in the database is 23.6 s, and the sampling frequency is 173.61 Hz. A total of 4 097 samples are recorded in each subset. In this paper, the BONN dataset is divided into 5 groups, namely A_N, A_F, A_S, B_Z, and B_O. Among them, subset A is derived from the data of healthy people, subset B is derived from the data of epilepsy patients.

Handling more dimensions and features increases the risk of overfitting, introduces noise and redundant information, and makes it harder for a model to learn and generalize accurately. To avoid this problem, feature selection methods are used to select the features that are most relevant to the seizure prediction task. Such as mean, standard deviation, peak value, approximate entropy, skewness, and PSD.

To evaluate the performance of the TDCBAM-SENet and avoid overfitting, the 5-fold cross validation technique and four indicators including accuracy (ACC), sensitivity (SEN), specificity (SPE), and false positive rate (FPR) are adopted. An Adam optimizer with a learning rate of 0.000 1 is used to minimize the loss function.

3.3 Analysis of experimental results

1) Performance analysis of TDCBAM-SENet and 2D CNN

Table 3 shows the ACC, SEN, SPE and FPR of TDCBAM-SENet are 98.33%, 98.88%, 98.45%, and 0.015 h^{-1}. This work is supported by the graphics processing unit (GPU), with memory consumption of about 3 GB. The average test time for each sample is about 3 h. However, the 2D CNN model achieves only ACC of 92.96%, SEN of 97.26%, SPE of 95.31%, and FPR of 0.069 h^{-1}. Therefore, TDCBAM-SENet has better results than the 2D CNN in 11 patients.

Among all patients, Chb01, Chb05, and Chb10 achieve very good results with ACC and SPE of over 99%, SEN of 100% and FPR of 0. The results of Chb04 are poor, with ACC of 93.35%, SEN of 96.73%, SPE of 97.04%, and FPR of 0.1. Table 4 shows the ACC, SPE and SEN of the method on the BONN dataset. The TDCBAM-SENet reaches good results with a learning rate of 0.000 1.

Table 3 Comparison of the prediction results of 2D CNN and TDCBAM-SENet on CHB-MIT dataset

No. patient	ACC/%		SEN/%		SPE/%		FPR/h^{-1}	
	2D CNN	TDCBAM-SENet	2D CNN	TDCBAM-SENet	2D CNN	TDCBAM-SENet	2D CNN	TDCBAM-SENet
Chb01	98.54	100.00	89.82	100.00	90.21	99.64	0.15	0.00
Chb02	88.56	97.53	98.19	97.71	97.45	97.39	0.17	0.02
Chb03	96.12	97.74	97.72	96.53	98.71	98.92	0.03	0.02
Chb04	93.35	96.73	93.33	97.04	92.33	99.00	0.10	0.06
Chb05	89.53	100.00	98.32	100.00	97.44	100.00	0.23	0
Chb07	97.12	98.34	99.21	100.00	99.34	97.32	0.01	0
Chb08	98.72	98.59	99.11	99.63	90.01	98.52	0.01	0.01
Chb10	91.21	100.00	100.00	100.00	98.67	99.87	0.00	0
Chb11	95.32	97.65	96.43	98.77	94.31	97.24	0.02	0.02
Chb21	89.89	98.32	99.23	98.56	98.27	96.31	0	0.01
Chb23	89.23	96.76	98.45	99.53	91.69	98.71	0.04	0.03

Table 4 TDCBAM-SENet results on the BONN dataset

Group	ACC/%		SEN/%		SPE/%	
	TDCBAM-SENet	2D CNN	TDCBAM-SENet	2D CNN	TDCBAM-SENet	2D CNN
A_N	100.0	98.8	100.0	99.8	99.8	98.3
A_F	100.0	98.9	100.0	100.0	100.0	99.2
A_S	100.0	98.2	99.9	99.7	99.6	98.9
B_Z	100.0	99.1	100.0	98.5	100.0	99.2
B_O	100.0	99.4	100.0	100.0	100.0	99.5

To analyze the performance of TDCBAM-SENet, inspired by the inception network structure, three sets of network models, G1, G2, G3 are set up, as shown in Table 5. Each group of networks consists of a 2D CNN and a TDCBAM-SENet, and is divided into groups 1 (G1), 2 (G2), and 3 (G3), the convolution kernel sizes of G1, G2, and G3 are set to 3×3, 5×5, and 7×7 respectively. C1, C2, and C3 represent the parameters of the 3-layer convolution of the network structure in G1, G2, and G3, respectively. Compared with 2D CNN, the same group of TDCBAM-SENet has CBAM and SE (CBAM-SE) blocks, namely CBAM-SE 1, CBAM-SE 2, and CBAM-SE 3. These six models perform the same seizure prediction task.

Table 5 Convolution kernel size of TDCBAM-SENet and 2D CNN in G1, G2, and G3

Structure	G1		G2		G3	
	2D CNN 1	TDCBAM-SENet 1	2D CNN 2	TDCBAM-SENet 2	2D CNN 3	TDCBAM-SENet 3
CBAM-SE 1	–	CBAM-SE	–	CBAM-SE	–	CBAM-SE
C1	3×3 32	3×3 32	5×5 32	5×5 32	7×7 32	7×7 32
C2	3×3 128	3×3 128	5×5 128	5×5 128	7×7 128	7×7 128
C3	3×3 128	3×3 128	5×5 128	5×5 128	7×7 128	7×7 128
CBAM-SE 2	–	CBAM-SE	–	CBAM-SE	–	CBAM-SE
C1	3×3 96	3×3 96	5×5 96	5×5 96	7×7 96	7×7 96
C2	3×3 96	3×3 96	5×5 96	5×5 96	7×7 96	7×7 96
C3	3×3 96	3×3 96	5×5 96	5×5 96	7×7 96	7×7 96
CBAM-SE 3	–	CBAM-SE	–	CBAM-SE	–	CBAM-SE

Due to the TDCBAM-SENet taking a long time to train on this dataset of 11 epilepsy patients. The patient Chb04 with the worst prediction results and Chb05 with the best prediction results are used to further train two types of models, the prediction results are shown in Tables 6 and 7.

Table 6 Prediction results of patient Chb04 in G1, G2, and G3

Model	ACC/%	SEN/%	SPE/%	FPR/h^{-1}
2D CNN 1	94.54	97.25	95.21	0.03
TDCBAM-SENet 1	97.67	98.78	98.22	0.02
2D CNN 2	92.14	94.47	89.11	0.02
TDCBAM-SENet 2	95.85	96.52	94.33	0.01
2D CNN 3	89.89	97.12	91.76	0
TDCBAM-SENet 3	93.11	99.87	97.65	0

Table 7 Prediction results of patient Chb05 in G1, G2, and G3

Model	ACC/%	SEN/%	SPE/%	FPR/h^{-1}
2D CNN 1	99.04	98.82	97.31	0.01
TDCBAM-SENet 1	99.80	100.00	98.63	0
2D CNN 2	97.67	97.86	95.91	0.01
TDCBAM-SENet 2	99.12	100.00	99.01	0
2D CNN 3	96.32	98.76	91.51	0.02
TDCBAM-SENet 3	98.67	99.45	97.57	0.01

Compared with 2D CNN 1, 2D CNN 2 and 2D CNN 3, the TDCBAM-SENet improves the ACC of 3.31%, 4.10%, 3.59% respectively on Chb04, and the the ACC of 0.76%, 1.48%, 2.43% respectively on Chb05. The SEN on Chb04 is increased by 1.57%, 2.17%, and 2.83%, and the SEN on Chb05 is increased by 1.19%, 2.19% and 0.70%, respectively. The TDCBAM-SENet improves the SPE of 3.16%, 5.86%, 6.42% respectively on Chb04, and the SPE of 1.36%, 3.23%, 6.62% respectively on Chb05. In addition, the FPR of the TDCBAM-SENet model for Chb04 and Chb05 are better than those of 2D CNN.

It can be seen that different hyperparameters have different effects on the learning effect of the model. Specifically, the TDCBAM-SENet 3 model's performance is relatively outstanding, especially, in terms of SEN, which can effectively capture and learn useful information. This shows that the TDCBAM-SENet 3 model has a superior ability to handle relevant tasks and make full use of key features in the data to improve overall performance. In the TDCBAM-SENet, by comparing and analyzing the performance of different network parameters, those parameter settings that could achieve relatively good results are chosen. Both 2D CNN and the TDCBAM-SENet use a 3D matrix as input. The experimental results show that, compared with 2D CNN, the CBAM module in the TDCBAM-SENet can fully extract the correlation information between channels contained in the 3D matrix and the spatial position information of electrode channels. Based on this information, the SE module can dynamically adjust the channel weight and optimize the performance of the model. This experiment evaluates the performance of different modules through validation sets to select the best model's hyperparameter settings.

2) Influence of training parameter

The hyperparameter settings of G1, G2 and G3 are a good way to show the differences between TDCBAM-SENet and 2D CNN. In the experiment, 80% of the dataset is set as training set and 20% as testing set. The prediction results of the TDCBAM-SENet and 2D CNN are shown in Fig. 9 and 10. Whether using Chb04 or Chb05 to train the model, the prediction accuracy of CBAM-SE 1, CBAM-SE 2, and CBAM-SE 3 keeps increasing when the training cycles are less than 100 times. When the training cycles are greater than 100 times, the accuracy no longer increases. However, the 2D CNN model has a slower convergence speed and larger fluctuation during training. Therefore, the TDCBAM-SENet model can effectively integrate channel attention and spatial domain information, and recalibrate the weights of different channels to improve the network's representation ability, thereby obtaining stronger learning ability compared to 2D CNN. In addition, the area under the curve (AUC) comparison experiments are also conducted, as shown in Fig. 11. The performance of the TDCBAM-SENet is better than the 2D CNN.

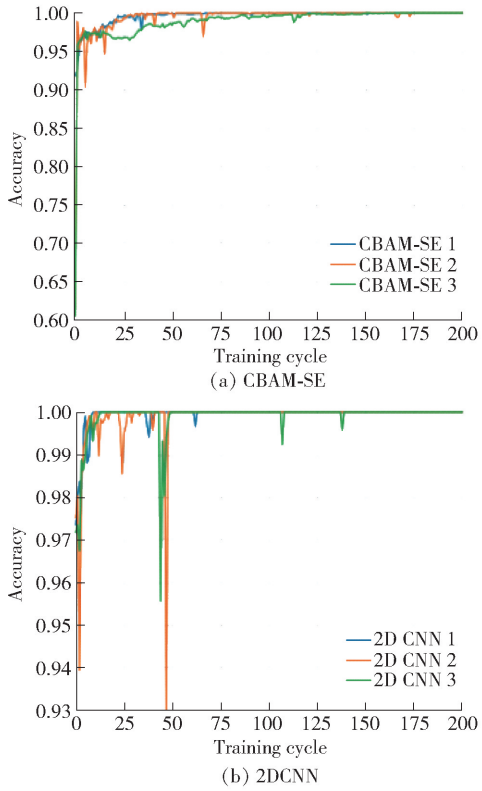

Fig. 9 Accuracy of differents models on the patient Chb04

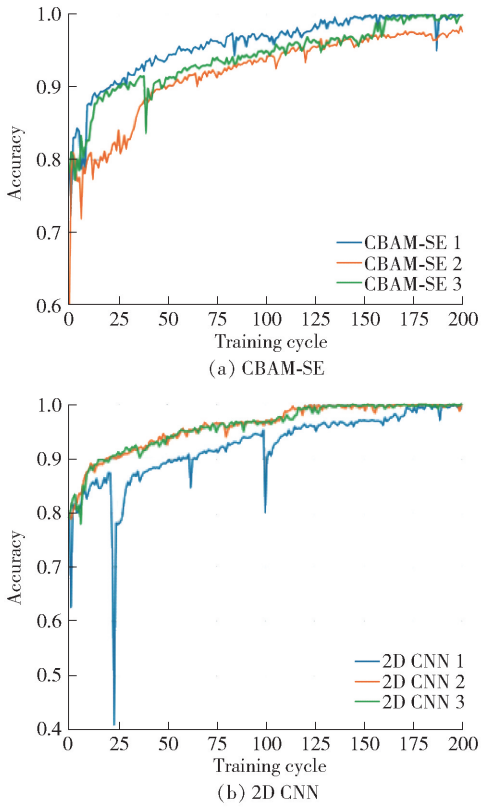

Fig. 10 Accuracy of different models on the patient Chb05

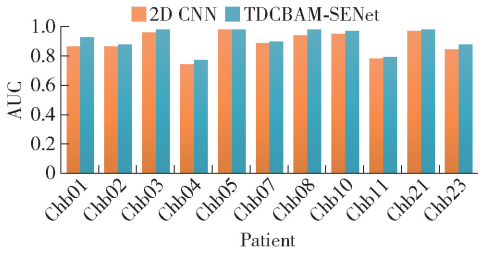

Fig. 11 Comparison of AUC between 2D CNN and TDCBAM-SENet

3) Advantage of 3D TF feature matrices

To demonstrate the advantage of the 3D TF feature matrix, the TDCBAM-SENet is also employed to deal with the time-domain features without permutation. The time-domain features also include mean, peak, standard deviation, skewness, approximate entropy, and PSD, which form a 2D feature matrix by 18 channels. Thus, the 2D feature matrix is 18 ×6 2D matrix.

The comparison results are shown in Table 8. Compared with the feature array, the 3D TF feature matrix has an ACC increase of 1.14%, SEN increase of 2.62%, and SPE increase of 1.91% in the time-domain, an ACC increase of 1.64%, SEN increase of 2.07%, and SPE decrease of 2.14% in the frequency-domain, and an ACC increase of 2.5%, SEN increase of 2.8%, and SPE increase of 2.82% in the TF domain. It has also achieved good results in other performance indicators. The results show that the performance of the 3D feature matrix is almost always better than that of the 2D feature matrix, regardless of which type of feature is used. The reason is that the 3D TF feature matrix contains spatial domain features and channel-related information. The spatial domain features obtained by analyzing the difference in signal characteristics of electrodes in different regions, can reflect the spatial relationships between different brain regions, thereby capturing the local features of brain electrical activity. By analyzing channel timing information, the dynamic changes between channels can be captured. These reveal the local characteristics of brain electrical activity and the interaction between different brain regions. By integrating these two pieces of information, a representation that is closer to the real cortical response can be obtained, thereby improving the performance of epilepsy prediction.

Table 8 Comparison results using time-domain, frequency-domain, and TF domain features for the 3D and 2D feature matrices

No. patient	ACC/%						SEN/%						SPE/%					
	Time-domain		Frequency-domain		TF domain		Time-domain		Frequency-domain		TF domain		Time-domain		Frequency-domain		TF domain	
	3D	2D	3D	2D	3D	2D	3D	2D	3D	2D	3D	2D	3D	2D	3D	2D	3D	2D
Chb01	99.4	99.1	98.2	90.2	100.0	99.2	100.0	100.0	98.4	93.3	100.0	100.0	99.5	98.6	90.3	92.1	99.6	99.2
Chb02	97.8	96.4	89.2	88.8	97.5	96.4	96.2	92.3	90.1	89.9	97.7	92.7	96.0	89.2	88.8	88.7	97.4	92.4
Chb03	96.4	93.2	89.4	88.5	97.7	92.3	97.3	96.3	92.1	88.8	96.5	90.3	98.3	96.7	90.1	92.1	98.9	92.1
Chb04	93.2	93.1	90.1	88.8	96.7	93.7	93.5	91.2	88.4	90.1	97.0	92.6	92.5	90.0	89.9	90.0	99.0	93.3
Chb05	96.0	97.2	95.4	98.2	100.0	97.6	97.2	93.3	92.4	97.7	100.0	99.7	95.1	90.1	90.1	89.7	100.0	98.5
Chb07	98.7	97.7	94.5	90.6	98.3	94.6	98.8	97.7	95.6	90.0	100.0	97.1	99.4	97.6	92.8	88.8	97.3	96.5
Chb08	99.0	95.4	93.0	91.2	98.6	98.0	98.4	91.1	94.4	90.2	99.6	99.1	91.4	91.4	91.7	93.4	98.5	98.4
Chb10	98.2	97.2	98.2	97.5	100.0	97.3	100.0	99.1	98.4	97.6	100.0	100.0	97.4	94.8	90.3	94.4	99.9	98.1
Chb11	96.5	97.1	89.9	89.9	97.7	97.6	98.3	95.6	92.4	89.9	98.8	97.5	93.4	97.6	91.1	87.7	97.2	97.7
Chb21	98.2	95.4	88.3	90.0	98.3	96.8	97.4	95.4	93.1	91.1	98.6	95.6	94.6	94.3	92.3	88.1	96.3	94.4
Chb23	94.4	93.3	95.2	91.9	96.8	92.1	99.4	97.6	94.5	90.3	99.5	93.8	97.8	94.4	89.9	92.3	98.7	92.2

4) Comparative analysis of TDCBAM-SENet components

Table 9 shows a comparison of the combined performance of patients selected from the CHB-MIT dataset on the TDCBAM-SENet model and model components. Among them, 2D CNN, 2D CNN with SE (2DCNN-SE) and 2D CNN with CBAM (2DCNN-CBAM) model components are selected according to Refs. [21, 30 – 31].

Table 9 Prediction results of TDCBAM-SENet component

Component	ACC/%	SEN/%	SPE/%	FPR/h^{-1}
2DCNN-SE[21]	93.94	95.56	96.75	0.073
2DCNN-CBAM[30]	96.95	98.40	98.13	0.017
2D CNN[31]	92.96	97.26	95.31	0.069
TDCBAM-SENet	98.33	98.88	98.45	0.015

Compared with 2D CNN, the performance of the 2DCNN-CBAM model shows significant improvement across all four indicators. This indicates that the CBAM module can effectively extract channel correlation information and channel spatial domain information from the 3D TF feature matrix. Compared with the 2DCNN-CBAM model, the performance of the TDCBAM-SENet shows further enhancement across all four indicators. This indicates that the SE module can dynamically optimize the weight of channels based on the channel correlation information and channel spatial domain information. In addition, the performance of the TDCBAM-SENet is also superior to the 2DCNN-SE. The reason may be that 2D CNN cannnot extract channel correlation information and channel spatial domain information from the 3D TF feature matrix. This restricts the role of the SE module in dynamically optimizing channel weights.

5) Comparative analysis of TDCBAM-SENet and existing network models

The performance of TDCBAM-SENet is compared with some existing researches. For all the compared studies, the CHB-MIT dataset, the BONN dataset, and the epilepsy state labeling prediction scheme are consistent. Tables 10 and 11 list the features and classifiers used in the comparative study. Among them, FLOP refers to the number of floating-point operations per second, which represents the time computational complexity of a model during the training process. The training time is the average of the training time recorded for 5 runs. For the CHB-MIT dataset, according to Refs. [4 – 6], traditional machine learning algorithms are used and good performance is achieved. However, the method combining STFT and deep models used in Refs. [30 – 33] is relatively poor. For the BONN dataset, Refs. [34 – 35]

conducted wavelet transform and on the signals, Refs. [36 – 37] used machine learning algorithms for signal processing. It can be seen that the TDCBAM-SENet is significantly superior to other methods in ACC, SEN, and SPE. This indicates that the 3D TF feature matrix and TDCBAM-SENet perform well in the epilepsy prediction task based on multi-channel EEG signals.

Table 10 Results of TDCBAM-SENet compared with other methods on CHB-MIT dataset

Method	ACC/%	SEN/%	SPE/%	FPR/h^{-1}	FLOP/G	Training time/s	Testing time/s
Convolutional autoencoder[4]	–	95.60	97.10	–	2.8	10.9	5.4
Bi-LSTM[5]	94.83	94.84	94.84	–	1.6	6.5	4,7
SVM[6]	95.93	–	94.97	0.04	0.6	14	6.3
CBAM[30]	97.95	98.40	–	0.02	21.2	4.6	3.2
Time-space domain[31]	–	92.94	–	0.07	1.6	4.6	2.1
STFT[32]	–	92.70	90.80	–	8.8	13.8	7.1
Redundancy analysis[33]	92.07	–	92.67	–	1.7	5.7	3.7
TDCBAM-SENet	98.27	98.81	98.32	0.01	0.3	3.8	1.8

Table 11 Results of TDCBAM-SENet compared with other methods on the BONN dataset

Method	ACC/%	SEN/%	SPE/%	FPR/h^{-1}	FLOP/G	Training time/s	Testing time/s
Continuous wavelet transform[34]	98.50	98.00	98.98	–	0.5	3.1	1.4
Random forest classifier[35]	99.65	98.06	100.00	–	0.7	4.1	3.3
CNN[36]	97.63	–	–	–	0.6	6.1	2.7
Wavelet transform[37]	98.44	97.50	98.38	–	0.3	4.3	2.3
TDCBAM-SENet	100.00	100.00	100.00	0.00	0.2	2.8	0.9

4 Conclusions

In this study, a seizure prediction method, TDCBAM-SENet was proposed. TDCBAM-SENet designs a 3D TF feature matrix that contains channel correlation information and channel spatial domain information, which uses the CBAM module to effectively capture the above information in the 3D feature matrix, uses SE module to dynamically optimize the weights of channels, thereby improving the performance of epilepsy prediction. The experiment on the datasets CHB-MIT and BONN shows that the TDCBAM-SENet has relatively high accuracy and sensitivity, which the error prediction rate is relatively low, and the overall performance is better than other methods.

To improve the generality of EEG data in patients with epilepsy, more subjects are needed in patients of different ages, clinical conditions, and disease characteristics. At the same time, with the growth of large-scale dataset and data sharing, collaborative researches across institutions and internationally will help build more comprehensive seizure prediction models, thereby improving the quality of life for people with epilepsy.

Acknowledgements

This work was supported by the National Natural Science Foundation of China (61872126, 62273290), the Fundamental Research Funds for the Central Universities (NSFRF1616), and the Programs for Science and Technology Development of Henan Province (222102210078).

References

[1] PRASANNA J, SUBATHRA M S P, MOHAMMED M A. et al. Automated epileptic seizure detection in pediatric subjects of CHB-MIT EEG database: a survey. Journal of Personalized Medicine, 2021, 11(10): Article 1028.

[2] MCCALLAN N, DAVIDSON S, NG K Y, et al. Epileptic multi seizure type classification using electroencephalogram signals from

the Temple University Hospital Seizure Corpus: a review. Expert Systems with Applications, 2023, 234: Article 121040.
[3] AFFES A, MDHAFFAR A, TRIKI C, et al. Personalized attention-based EEG channel selection for epileptic seizure prediction. Expert Systems with Applications, 2022, 206: Article 117733.
[4] SUN B A, LV J J, RUI L G, et al. Seizure prediction in scalp EEG based channel attention dual-input convolutional neural network. Physica A: Statistical Mechanics and its Applications, 2021, 584: Article 126376.
[5] MA Y H, HUANG Z T, SU J Y, et al. A multi-channel feature fusion CNN-Bi-LSTM epilepsy EEG classification and prediction model based on attention mechanism. IEEE Access, 2023, 11: 62855 – 62864.
[6] ZHONG L, WAN J, YI F, et al. Epileptic prediction using spatiotemporal information combined with optimal features strategy on EEG. Frontiers in Neuroscience, 2023: Article 17.
[7] FEIZBAKHSH B, OMRANPOUR H. Cluster-based phase space density feature in multichannel scalp EEG for seizure prediction by deep learning. Biomedical Signal Processing and Control, 2023, 86(C): Article 105276.
[8] RA J S, LI T N, LI Y. A novel epileptic seizure prediction method based on synchroextracting transform and 1-dimensional convolutional neural network. Computer Methods and Programs in Biomedicine, 2023, 240: Article 107678.
[9] OZCAN A R, ERTURK S. Seizure prediction in scalp EEG using 3D convolutional neural networks with an image-based approach. IEEE Transactions on Neural Systems and Rehabilitation Engineering, 2019, 27(11): 2284 – 2293.
[10] XU X, ZHANG Y, ZHANG R H, et al. Patient specific method for predicting epileptic seizures based on DRSN-GRU. Biomedical Signal Processing and Control, 2023, 81: Article 104449.
[11] LI C, HUANG X Y, SONG R C, et al. EEG-based seizure prediction via transformer guided CNN. Measurement, 2022, 203: Article 111948.
[12] SHI Z Z, LIAO Z Q, TABATA H. Enhancing performance of convolutional neural network based epileptic electroencephalogram diagnosis by asymmetric stochastic resonance. IEEE Journal of Biomedical and Health Informatics, 202, 27(9): 4228 – 4239.
[13] ZHANG S S, CHEN D, RANJAN R, et al. A lightweight solution to epileptic seizure prediction based on EEG synchronization measurement. Journal of Supercomputing, 2021, 77(4): 3914 – 3932.
[14] EIN SHOKA A, DESSOUKY M M, EL-SAYED A, et al. An efficient CNN based epileptic seizures detection framework using encrypted EEG signals for secure telemedicine applications. Alexandria Engineering Journal, 2023, 65: 399 – 412.
[15] WANG Y, SHI Y F, CHENG Y L, et al. A spatiotemporal graph attention network based on synchronization for epileptic seizure prediction. IEEE Journal of Biomedical and Health Informatics, 2023, 27(2): 900 – 911.
[16] ZHANG T, WANG X H, XU X M, et al. GCB-Net: graph convolutional broad network and its application in emotion recognition. IEEE Transactions on Affective Computing, 2022, 13(1): 379 – 388.
[17] WANG M, EL-FIQI H, HU J K, et al. Convolutional neural networks using dynamic functional connectivity for EEG-based person identification in diverse human states. IEEE Transactions on Information Forensics and Security, 2019, 14(12): 3259 – 3272.
[18] CHEN X, ZHENG Y J, DONG C X, et al. Multi-dimensional enhanced seizure prediction framework based on graph convolutional network. Frontiers in Neuroinformatics, 2021, DOI: 10.3389/fninf.2021.605729.
[19] DISSANAYAKE T, FERNANDO T, DENMAN S, et al. Geometric deep learning for subject independent epileptic seizure prediction using scalp EEG signals. IEEE Journal of Biomedical and Health Informatics, 2022, 26(2): 527 – 538.
[20] ZHONG P X, WANG D, MIAO C Y. EEG-based emotion recognition using regularized graph neural networks. IEEE Transactions on Affective Computing, 2022, 13(3): 1290 – 1301.
[21] LI Y, LIU Y, CUI W G, et al. Epileptic seizure detection in EEG signals using a unified temperal-spectral squeeze-and-excitation network. IEEE Transactions on Neural Systems and Rehabilitation Engineering, 2020, 28(4): 782 – 794.
[22] LI C, DENG Z W, SONG R C, et al. EEG-based seizure prediction via model uncertainty learning. IEEE Transactions on Neural Systems and Rehabilitation Engineering, 2023, 31: 180 – 191.
[23] LIU S, WANG J, LI S S, et al. Epileptic seizure detection and prediction in EEGs using power spectra density parameterization. IEEE Transactions on Neural Systems and Rehabilitation Engineering, 2023, 31: 3884 – 3894.
[24] CHAO H, DONG L, LIU Y L, et al. Emotion recognition from multiband EEG signals using CapsNet. Sensors, 2019: 19(9): Article 2212.
[25] WANG Y F, CUI W G, YU T, et al. Dynamic multi-graph convolution based channel-weighted transformer feature fusion network for epileptic seizure prediction. IEEE Transactions on Neural Systems and Rehabilitation Engineering, 2023, 31: 4266 – 4277.
[26] BAKR E M, EL-SALLAB A, RASHWAN M. EMCA: efficient multiscale channel attention module. IEEE Access, 2022, 10: 103447 – 103461.
[27] SAMEE N A, MAHMOUD N F, ALDHAHRI E A, et al. RNN and BiLSTM fusion for accurate automatic epileptic seizure diagnosis using EEG signals. Life, 2022, 12(12): Article 1946.
[28] ZHANG X X, SHE Q S, TAN T C, et al. Multi-source geometric metric transfer learning for EEG classification. Biomedical Signal Processing and Control, 2023, 81: Article 104435.
[29] LIU C L, XIAO B, HSAIO W H, et al. Epileptic seizure prediction with multi-view convolutional neural networks. IEEE Access, 2019, 7: 170352 – 170361.
[30] LU X, WEN A H, SUN L, et al. An epileptic seizure prediction method based on CBAM-3D CNN-LSTM model. IEEE Journal of Translational Engineering in Health and Medicine, 2023, 11: 417 – 423.
[31] GAO Y K, LIU A P, WANG L L, et al. A self-interpretable deep learning model for seizure prediction using a multi-scale prototypical part network. IEEE Transactions on Neural Systems and Rehabilitation Engineering, 2023, 31: 1847 – 185.

To p. 100

PFCM and recurrent neural network-based intrusion detection system for cloud environment. International Journal of Business Intelligence and Data Mining, 2019, 14(4): 504 – 527.

[26] FU Y S, LOU F, MENG F Z, et al. An intelligent network attack detection method nased on RNN. Proceedings of the IEEE 3rd International Conference on Data Science in Cyberspace (DSC'18), 2018, Jun 18 – 21, Guangzhou, China. Piscataway, NJ, USA: IEEE, 2018: 483 – 489.

[27] SHANG W L, SHI H, ZHAO J M, et al. An anomaly detection method of process data based on SAE-LSTM. Acta Electronica Sinica, 2021, 49(8): 1561 – 1568 (in Chinese).

[28] KASONGO S M, SUN Y X. A deep gated recurrent unit based model for wireless intrusion detection system. ICT Express, 2021, 7(1): 81 – 87.

[29] XU C Y, SHEN J H, DU X, et al. An intrusion detection system using a deep neural network with gated recurrent units. IEEE Access, 2018, 6: 48697 – 48707.

[30] ZHANG X L, YIN S L. Intrusion detection model of random attention capsule network based on variable fusion. Journal on Communications, 2020, 41(11): 160 – 168 (in Chinese).

[31] YIN S L, ZHANG X L, ZUO L Y. Intrusion detection system for dual route deep capsule network. Journal of Computer Research and Development, 2022, 59(2): 418 – 429 (in Chinese).

[32] ZHANG X L, YIN S L. Intrusion detection model of random attention capsule network based on variable fusion. Journal on Communications, 2020, 41(11): 160 – 168 (in Chinese).

(Editor: Wang Xuying)

From p. 69

[32] USMAN S M, KHALID S, ASLAM M H. Epileptic seizures prediction using deep learning techniques. IEEE Access, 2020, 8: 39998 – 40007.

[33] YANG X W, ZHAO J Q, SUN Q, et al. An effective dual self attention residual network for seizure prediction. IEEE Transactions on Neural Systems and Rehabilitation Engineering, 2021, 29: 1604 – 1613.

[34] TURK Ö, ÖZERDEM M S. Epilepsy detection by using scalogram based convolutional neural network from EEG signals. Brain Sciences, 2019, 9(5): Article 115.

[35] RASHED-AL-MAHFUZ M, MONIM A, UDDIN S, et al. A deep convolutional neural network method to detect seizures and characteristic frequencies using epileptic electroencephalogram (EEG) data. IEEE Journal of Translational Engineering in Health and Medicine, 2021, 9: Article 2000112.

[36] SUKRITI, CHAKRABORTY M, MITRA D. A computationally efficient automated seizure detection method based on the novel idea of multiscale spectral features. Biomedical Signal Processing and Control, 2021, 70: Article 102990.

[37] ZHAO W, ZHAO W B, WANG W F, et al. A novel deep neural network for robust detection of seizures using EEG signals. Computational and Mathematical Methods in Medicine, 2020, DOI: 10.1155/2020/9689821.

(Editor: Wang Xuying)